ADVANCED ENERGY MATERIALS
www.advenergymat.de

Static and Dynamic Disorder of Charge Transfer States Probed by Optical Spectroscopy

*Frank-Julian Kahle, Alexander Rudnick, Stefan Wedler, Rishabh Saxena, Robin Ammenhäuser, Ullrich Scherf, Sergey Bagnich, Heinz Bässler, and Anna Köhler**

Since the key role of charge transfers (CT) states has been identified for organic solar cells (OSCs), research into their properties is a timely topic. Conventionally, their absorption and emission spectra are described in terms of Marcus' electron transfer theory. This is a single site approach with the essential parameter being the reorganization energy. Thus, it ignores ensemble effects, notably the role of static disorder that is inevitably present in a spin-coated OSC film. Here time dependent photoluminescence spectroscopy is applied on blends of the polymeric donor MeLPPP with either the non-fullerene acceptor SF-PDI$_2$ or with PC$_{61}$BM within a temperature range from 295 to 5 K. The authors monitor how initially excited singlet states are converted to emissive CT states. Concomitantly, emission from residual singlets on the acceptor is observed rather than hybrid CT-states. The role of spectral diffusion in this process is discussed. From the temperature and time dependent linewidths of absorption, fluorescence, and CT emission, the static and dynamic contributions to the total disorder are inferred. In both blends, at 295 K, the contribution of static disorder is comparable to the dynamic disorder.

1. Introduction

Upon exciting either the donor or the acceptor in an organic solar cell (OSC) a pair of charges is generated that is—wishfully—collected at the electrodes. This process is sequential. Initially a coulomb bound electron–hole pair is created that can either fully dissociate or suffer geminate recombination. It was a highly disputed question whether or not this process requires a driving force set up by the offset of the ionization potentials or electron affinities at the interface between donors and acceptors. The work of Vandewal et al. provided a clear answer to this question.[1,2] These authors measured the internal quantum efficiency (IQE) of an OSC over a broad spectral range encompassing the absorption spectrum of the charge transfer (CT) state of the donor and acceptor. They found that the IQE is basically independent of photon energy. This has an important consequence. It implies that the dissociating entity is the cold CT state of donor and acceptor and does not require driving force for its generation.[3,4] This does not rule out that a more expanded electron–hole pair may initially be generated but it indicates that the vast majority of such "hot" electron–hole-pairs relax to cold states within the coulomb well before they execute a random walk to escape from it.[1,2,5–12] The crucial entity in the dissociation process is therefore the CT state of the donor–acceptor couple and to unravel its properties is an important issue.[13,14] The usual formalism to describe the dynamics of CT states rests upon the classic Marcus theory of electron transfer[15] and its extension by Levich, Jortner, and Marcus.[16–18] The crucial parameter in this theory is the reorganization energy λ that is associated with electron transfer. This formalism is a single site approach, appropriate for chromophores in dilute solution as confirmed by the work of Gould et al.[19] and others.[20–22] It is open to conjecture, though, whether or not this approach is sufficient to analyze CT spectra in a condensed phase because there the pertinent energies are no longer well-defined but are subject to a distribution that reflects the random variation of the van der Waals coupling of an excited chromophore with its polarizable environment giving rise to static disorder.[23–26] Static disorder is, for instance, one reason why the mobility of charge carriers in organic semiconductor films is much lower than in their crystalline counterparts except under field-effect-transistor operation.[27–32]

F.-J. Kahle, A. Rudnick, S. Wedler, R. Saxena, S. Bagnich, A. Köhler
Soft Matter Optoelectronics
Universität Bayreuth
Universitätsstr. 30, 95447 Bayreuth, Germany
E-mail: anna.koehler@uni-bayreuth.de
R. Ammenhäuser, U. Scherf
Macromolecular Chemistry Group (BUWMakro) and Wuppertal Institute for Smart Materials and Systems (CM@S)
Bergische Universität Wuppertal
Gauss-Str. 20, 42119 Wuppertal, Germany
H. Bässler, A. Köhler
Bayreuth Institute of Macromolecular Research (BIMF)
Universität Bayreuth
95447 Bayreuth, Germany
A. Köhler
Bavarian Polymer Institute (BPI)
Universität Bayreuth
95448 Bayreuth, Germany

The ORCID identification number(s) for the author(s) of this article can be found under https://doi.org/10.1002/aenm.202103063.

DOI: 10.1002/aenm.202103063

In order to implement the effect of static disorder into the description of CT states in OSCs, Burke et al.[33] proposed that the term $\frac{\sigma^2}{2k_BT}$ should be added in addition to the reorganization energy, where σ^2 is the variance of the Gaussian distribution of the density of states (DOS). In our recent work on the spectroscopy of a MeLPPP:$PC_{61}BM$ blend we analyzed CT states and conclude that static disorder is indeed necessary for their correct description.[34] However, Tvingstedt et al.[35] and more recently Göhler et al.[36] as well as Panhans et al.[37] criticized this conclusion and argue that static disorder is unimportant to explain the properties in an OSC. One of the arguments[36] is that the peak of the CT-emission spectrum in a selected TAPC:C_{60} blend does not noticeably shift when the device is cooled down to 125 K, contrary to what the $\frac{\sigma^2}{2k_BT}$ term predicts. This would imply that indeed the Marcus-type single site approximation is enough to explain the dynamics of CT states in OSC operation. However, this notion of a single site approximation is in conflict with the work by Melianas et al.[38] who stress that the CT states, generated by the recombination of electrons and holes in an OSC operated under forward bias, suffered a long journey and are therefore not well-defined entities but depend on the way how they are been generated. Similarly, it conflicts with Upreti and coworkers[39] who emphasize the role of the disorder-broadened DOS in the value of the open-circuit voltage.

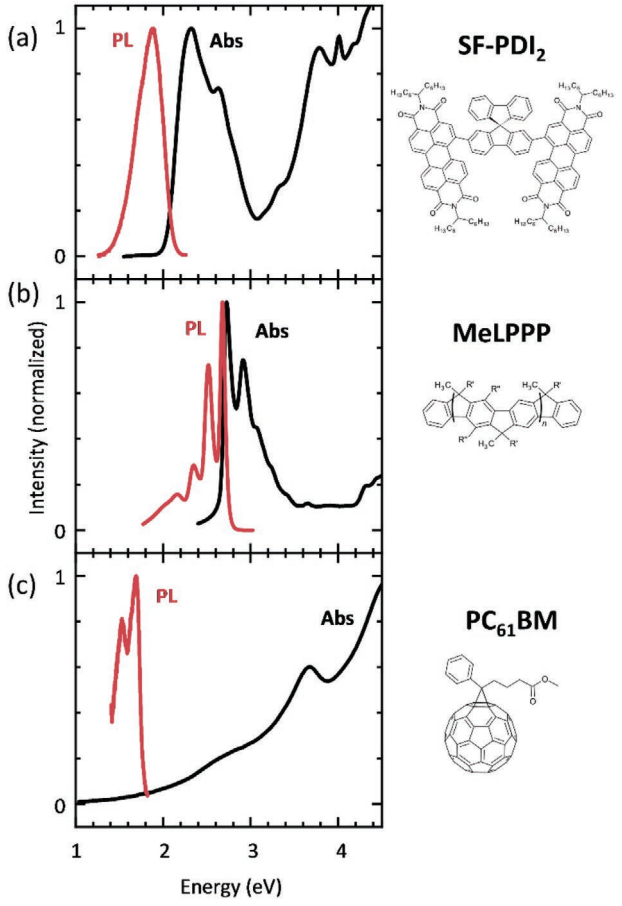

Figure 1. Thin film absorption and emission spectra and chemical structures of a) SF-PDI_2, b) MeLPPP, and c) $PC_{61}BM$.

This controversy prompted us to investigate CT states in a MeLPPP:SF-PDI_2 blend and to analyze data on the CT states in a MeLPPP:$PC_{61}BM$ blend that had been taken in the course of our study by Kahle et al.[34] For reference, **Figure 1** shows the chemical structures of these three compounds, along with their steady state absorption and emission spectra. SF-PDI_2 is a non-fullerene acceptor (NFA) in OSCs and its fluorescence (FL) spectra are significantly broader than those of $PC_{61}BM$. This broader DOS should allow delineating disorder effects. We select MeLPPP as a donor material that has been spectroscopically well characterized[40] and has a comparatively low lying ionization potential level around −5.75 eV.[41] The CT emission is therefore in a conveniently accessible spectral range (1.5–1.6 eV), and non-radiative decay, controlled by the gap law,[42,43] is less important. We are aware that MeLPPP is not a preferred donor material in the OSC community due to its large optical gap. However, our aim is not to optimize solar cell efficiency. Rather, we aim to conduct an exemplary study of the properties of a CT state involving a NFA and to compare it to the results for fullerene acceptors. We employ time dependent photoluminescence (PL) spectroscopy covering a temperature range from 295 to 5 K in order to delineate how fluorescence as well CT emission from neat and blended films evolve with time, thereby drawing upon the phenomenon of spectral diffusion. Spectral diffusion is a phenomenon that reflects the motion of an excited state, be it a charge or an exciton, within an energetically dispersed DOS distribution, and is therefore an unambiguous probe of static disorder.[44–50] From the evolution of gated PL spectra of a neat SF-PDI_2 film and the spectra of MeLPPP:SF-PDI_2 and MeLPPP:$PC_{61}BM$ blends in the temperature range between 295 and 5 K we can explore how CT states are created by optical excitation and how they decay. From the temperature dependence of the absorption and emission band widths we determine the standard deviations of the Gaussian distributions (σ) and the related variances (σ^2). We find that, upon cooling, the emission profiles of the CT states in the blends become more narrow, yet this saturates below 100 K. The ratio between the room temperature values of the variances for static and dynamic disorder in the CT state is roughly 1:2 (MeLPPP with $PC_{61}BM$) or 3:2 (MeLPPP with SF-PDI_2). The dynamic disorder comprises both temperature-independent and temperature-dependent electron–phonon coupling. This shows that in these systems static disorder of CT states constitutes a major contribution. The experiments also delineate the role of spectral diffusion in the formation of CT states and demonstrate that in a bulk system, like an OSC, a single site approximation is insufficient for analyzing CT states.

2. Results

2.1. Absorption and Fluorescence Spectra of SF-PDI_2

Figure 2a shows the steady state-absorption and FL spectra of SF-PDI_2 in toluene solution at room temperature. The spectra are inhomogeneously broadened with a barely detectable vibronic structure. The peaks of the S_1–S_0 absorption and the emission

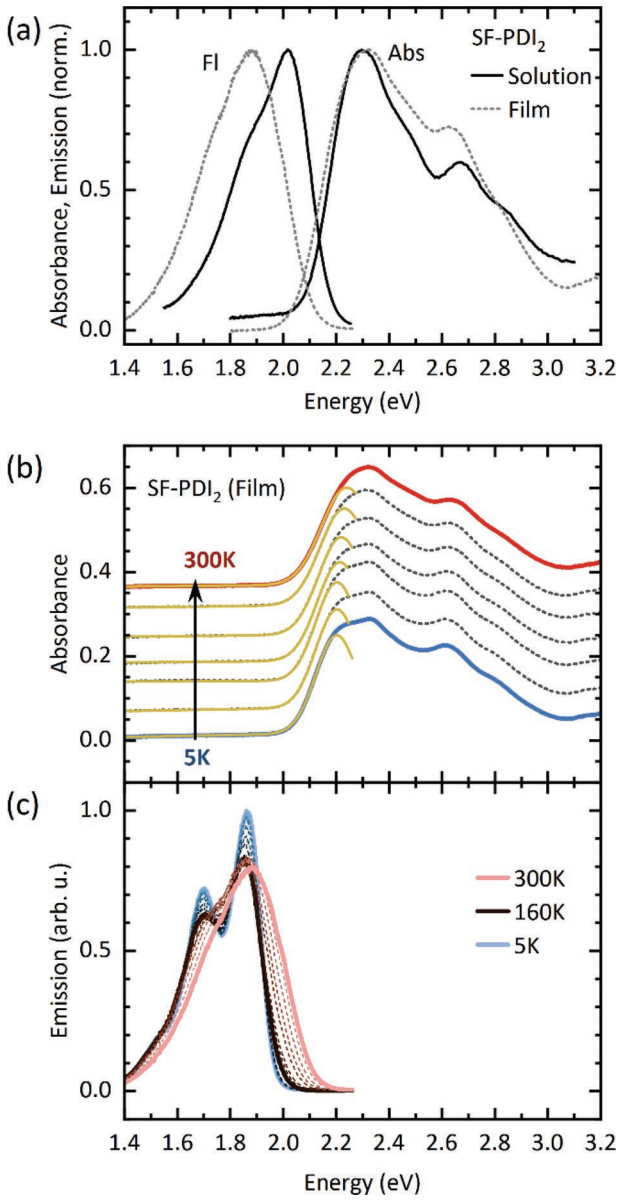

Figure 2. a) Normalized absorption and steady state fluorescence of SF-PDI$_2$ at 295 K in toluene solution and as thin film. b) Absorption of a SF-PDI$_2$ thin film between 300 and 5 K in steps of 50 K. Yellow lines indicate Gaussian fits of the low energy side and the spectra are vertically offset for clarity. c) Steady state fluorescence of a SF-PDI$_2$ thin film between 300 and 5 K in steps of 20 K.

features are at 2.30 and 2.02 eV, respectively. The origin of the transition, inferred from the crossing point between absorption and emission, is at 2.13 eV and the Stokes' shift between the absorption and emission 0–0 transition peaks is 0.28 eV.

Upon film formation, there is almost no spectral shift of the absorption spectrum. The dominant feature of the S_1–S_0 transition is a superposition of two inhomogeneously broadened features split apart by about 100 meV (Figure 2b). Upon sample cooling the leading edge of the absorption spectra become slightly narrower and bears out a minor bathochromic shift.

Figure 2c shows how the FL spectrum of a SF-PDI$_2$ film evolves when the temperature decreases from 295 to 5 K. While the absorption spectra of solution and film are basically iso-energetic, the FL spectrum of the film is shifted to the red by about 150 meV and becomes significantly narrower upon sample cooling. To quantify the temperature dependence of the peak positions of the absorption and FL features as well as of the line widths, the spectra have been subjected to a spectral analysis using Gaussian envelope functions. We found that the absorption peak continuously shifts to the red upon sample cooling while the emission peak passes through a minimum as shown in **Figure 3**a. This minimum is a signature of frustrated spectral diffusion that can occur for molecular films when the Förster radius is small, as detailed further below. The associated Stokes' shift between absorption and emission shows a maximum around 250 K (Figure 3b). The width of the absorption band, quantified in terms of their standard deviations (σ) of the

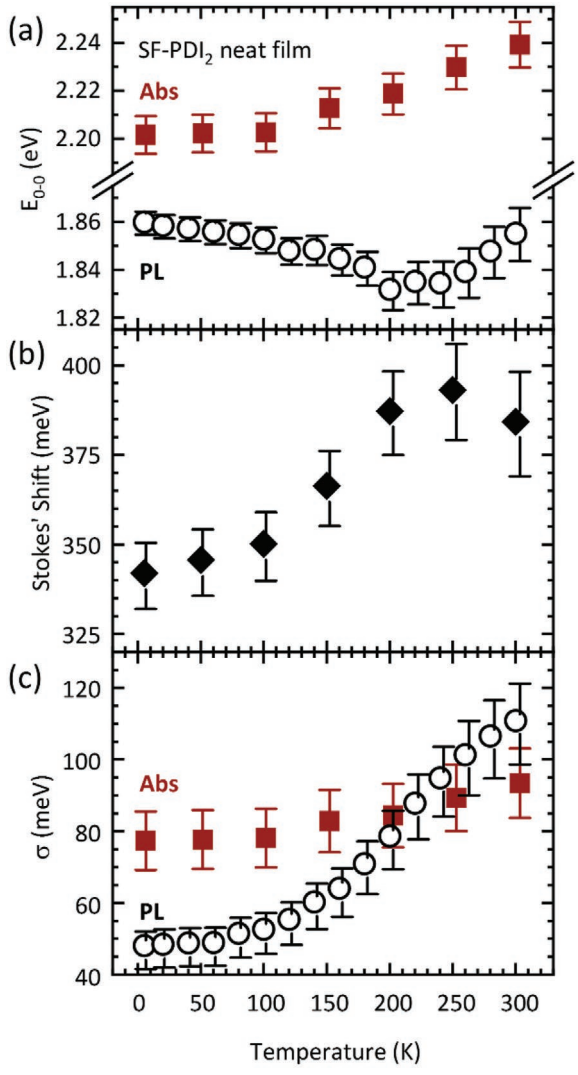

Figure 3. a) Transition energy, b) corresponding Stokes' shift, and c) Gaussian linewidth of a SF-PDI$_2$ film as a function of temperature for absorption (solid squares) and emission (open circles) extracted from Gaussian fits.

associated Gaussian line widths, decreases moderately from 95 to 80 meV upon sample cooling, while in emission σ drops substantially from 110 meV at 295 K to 48 meV at 5 K (Figure 3c).

The fact that the Stokes' shift, that is, the energy difference between the experimentally observed absorption and FL 0–0 peak maxima, almost doubles when going from dilute solution to film is an indication that singlet excitons in a SF-PDI$_2$ film are subject to spectral diffusion. In order interpret the film spectra we will therefore briefly outline the concept of spectral diffusion. It is a ubiquitous and well-established phenomenon in studies of fluorescence and phosphorescence of non-crystalline organic semiconductors,[45,50] and it is related to inhomogeneous line broadening caused by static disorder. To quantify the effect, it appears useful to briefly recall central aspects of the dynamics of excitations in a dense disordered medium.

In an organic semiconductor, elementary excitations such as charge carriers, singlet excitons, and triplet excitons execute a random walk among sites within a DOS distribution which is usually of Gaussian shape, characterized by a standard deviation σ. Upon broadband illumination excitations are generated randomly within this DOS distribution and execute a random walk, thereby relaxing within the DOS distribution. This relaxation process proceeds on a logarithmic timescale and can be monitored by gated spectroscopy. The process proceeds until thermal equilibrium energy is reached when the transfer steps down and up in energy become balanced. Random walk theory predicts that under quasi-equilibrium the center of the occupied DOS is at σ_{stat^2}/kT below of the center of the original DOS. This temperature dependent relaxation process is a result of the broad DOS distribution, that is, the static disorder, and it contributes to the Stokes' shift. Another contribution arises from the dynamic disorder, that is, intramolecular and intermolecular geometric reorganization (phonon-induced broadening). This includes thermally activated librations and rotations of the molecular structure as well as intermolecular motions. In general, the cumulated Stokes shift is the sum of the relaxation energies due to dynamic disorder and static disorder.

Eventually, spectral diffusion is terminated by the lifetime of the excitations, that is, singlet or triplet excitons, regardless whether the energetic relaxation has come to the thermal equilibrium value of $\sigma_{stat}{}^2/kT$ below the center of the DOS or not. An experimental signature of this effect is that FL or phosphorescence spectra of a bulk film of chromophores (even rigid chromophores) initially bear out red-shift upon sample cooling yet this shift saturates below a critical temperature T_c.[51,52] Below this T_c, the excitation decays before the thermal equilibrium energy is reached. The condition that this saturation happens depends on the coupling strength between the chromophores and the lifetime of the excitations. In the case of diffusion by a series of Förster transfer steps, this balance is expressed through the Förster radius. For most organic semiconductors, the relaxation process by spectral diffusion reaches thermal equilibrium during the lifetime of the excitation when the required energy shift, that is, $\sigma_{stat}{}^2/kT$, is smaller than $x \cdot \sigma_{stat}$, with the empirical value $x \approx 3 \pm 1$.[51,52] This translates into a critical temperature of $T_c \approx \sigma_{stat}/xk$ below which spectral diffusion saturates at a constant value. It implies that the energetic position of emission spectra with σ_{stat} above about 70 meV should be more or less insensitive to temperature below 295 K. This is very important for spectral analysis. If one ignores the (temperature dependent) spectral relaxation in a condensed phase, one would erroneously associate the entire Stokes' shift ΔE with dynamic disorder, thus overestimating its value. In summary,

$$\Delta E = E_{0-0}^{Abs} - E_{0-0}^{PL} = \lambda_{abs} + \lambda_{Fl} + \sigma_{stat}^2/kT;\ T \geq T_c \quad (1)$$

with $T_c \approx \sigma_{stat}/xk$, $x \approx 3 \pm 1$. λ, that is, λ_{Fl} or λ_{abs}, is the phonon-controlled reorganization energy due to dynamic disorder in the ground state geometry (λ_{abs}) or in the excited state equilibrium geometry (λ_{Fl}). It is worth emphasizing that we are considering the differences between the experimentally observed "0–0" transition energies in absorption and emission, where "0" refers to the absence of high frequency modes. Thus, λ here is not associated with the change in equilibrium geometry due to coupling to high-frequency vibrations ($\hbar\omega > 100$ meV). Rather, as already mentioned, it reflects the contributions of inter- or intramolecular low-frequency phonons ($\hbar\omega < 10$ meV) to the line width. σ_{stat} refers to the DOS involved in emission. Equation (1) does not take into account any effects from frustrated spectral diffusion, that is, the freezing out of the relaxation process sometimes observed below T_c.[51]

Based upon this concept we will analyze the absorption and FL spectra of a SF-PDI$_2$ film, considering that variances of static and dynamic contributions to the Gaussian line width add up linearly according to[25,53]

$$\sigma_{tot}^2 = \sigma_{stat}^2 + \sigma_{dyn}^2 \quad (2)$$

Using the data from Figure 3c we plot the σ value on a σ^2 versus T scale (**Figure 4**).This allows us to differentiate between the contributions that are thermally activated and those that are not. The 0 K limit comprises the contributions from the static disorder, σ_{stat}, and the temperature-independent contributions from the electron–phonon coupling. We shall refer to this latter contribution as $\sigma_{dyn,0K}$. The difference between the measured linewidth in the 0 K limit and the measured linewidth at a given temperature results from the thermally activated part of the electron–phonon coupling that we refer to as $\sigma_{dyn,th}$. Thus, the overall dynamic disorder, that is, the disorder

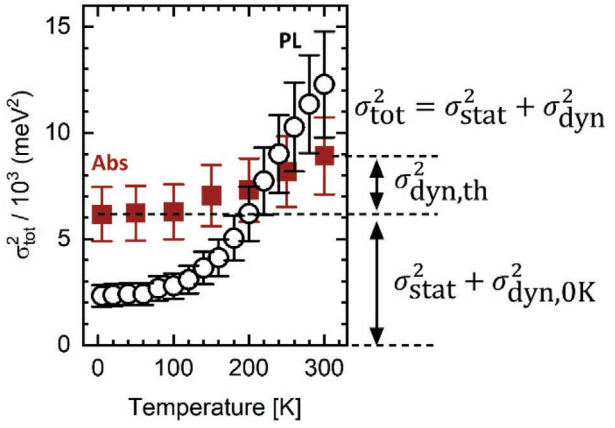

Figure 4. Squared Gaussian linewidths σ^2 measured for a film of SF-PDI$_2$ as a function of temperature. The static and dynamic contribution to the total value is illustrated on the right.

Table 1. The experimentally determined disorder values at 300 and 0 K.

	$\sigma^2_{tot}(300\ K)$ [10^3 (meV)^2]	$\sigma^2_{dyn,0K}+\sigma^2_{stat}$ [10^3 (meV)^2]	$\sigma^2_{dyn,th}(300\ K)$ [10^3 (meV)^2]
SF-PDI$_2$ S1 Abs in neat film	8.9 ± 1.8	6.2 ± 1.3	2.7 ± 2.2
SF-PDI$_2$ S1 PL in neat film	12.3 ± 2.5	2.3 ± 0.5	10.0 ± 2.5
SF-PDI$_2$ S1 Abs in MeLPPP:SF-PDI$_2$,	10.4 ± 2.1	7.0 ± 1.4	3.4 ± 2.5
CT state PL in MeLPPP:SF-PDI$_2$	9.6 ± 2.0	8.5 ± 1.7	1.1 ± 1.1
CT state PL in MeLPPP:PC$_{61}$BM	5.9 ± 1.2	3.6 ± 0.8	2.3 ± 1.4

resulting from the coupling to phonon modes, consists of a temperature-independent and a temperature-dependent part, $\sigma^2_{dyn} = \sigma^2_{dyn,0K} + \sigma^2_{dyn,th}$.

If we apply this to the data shown in Figure 4 we find for the linewidth in absorption a temperature-independent part $\sigma^2_{dyn,0K} + \sigma^2_{stat} = 6200\,(meV)^2$ and a temperature dependent part of $\sigma^2_{dyn,th} = 2700\,(meV)^2$ at 300 K, which combine to a total linewidth of $\sigma^2_{tot} = 8900\,(meV)^2$. Thus we obtain $\sqrt{\sigma^2_{dyn,0K}+\sigma^2_{stat}}$ = 79 meV and $\sigma_{dyn,th}$(300 K) = 52 meV. We can apply the same approach to the fluorescence and obtain the values summarized in **Table 1** further below, that is, $\sqrt{\sigma^2_{dyn,0K}+\sigma^2_{stat}}$ = 48 meV and $\sigma_{dyn,th}$(300 K) = 100 meV. When considering the values obtained from fluorescence rather than absorption, it is a good idea to keep in mind that fluorescence, notably at low temperatures, usually takes place before thermal equilibrium in the DOS is reached. Thus, the values for σ_{stat} are underestimated, and in consequence those for $\sigma_{dyn,th}$ are overestimated.

The experimentally observed variances of the FL linewidth are significantly lower than those of absorption and approach an asymptotic value of 2300 (meV)^2 ($\sqrt{\sigma^2_{dyn,0K}+\sigma^2_{stat}}$ = 48 meV). A lower linewidth in emission than in absorption is common and is a signature that spectral diffusion has not yet completed to the equilibrium value prior to radiative decay. For example, in a film of MEH-PPV, the observed S_1–S_0 0–0 transition has a Gaussian width of $\sqrt{\sigma^2_{dyn,0K}+\sigma^2_{stat}}$ = 75 meV in absorption, yet of $\sqrt{\sigma^2_{dyn,0K}+\sigma^2_{stat}}$ = 42 meV in emission.[54] The reason is that the hopping rate for excitations, and thus the rate of spectral diffusion is not uniform across the DOS. Spectral diffusion proceeds by a sequence of resonant energy transfer events. A resonance condition between the energy donating and accepting site is easily met in the center of the DOS so that downhill jumps are fast, yet for donating states in the tail, suitable acceptor sites are further apart, which slows down the transfer. As a result, the DOS distribution narrows. Monte Carlo simulations, detailed in Figure S1, Supporting Information support this reasoning and demonstrate that the width of the emitting sites has a standard deviation σ_{stat} that is about 2/3 of that of the absorbing sites.

Experiments on a neat film, performed in the gated detection mode, provide further information on the time dependence of the FL decay. **Figure 5** shows that there is prompt fluorescence followed by delayed fluorescence (DF) after roughly 100 ns. At room temperature, the prompt component has a life time of ≈12 ns and increases to 26 ns at 5 K. (Figure 5b,c). The fact the DF does not vanish upon cooling to 5 K implies that it originates from triplet–triplet-annihilation rather from thermally activated triplet activation as in thermally activated DF (TADF). These data serve as reference for the data obtained on the blend films and will be discussed alongside the results on the blends.

2.2. Absorption and Photoluminescence of a MeLPPP:SF-PDI$_2$ Blend

Having analyzed the absorption and FL spectra in a neat SF-PDI$_2$ film we now explore how blending of SF-PDI$_2$ with MeLPPP affects the absorption and the PL. It turns out that within a spectral range of 2.0 to 2.5 eV, the absorption spectrum of the blend film is no different to that of a neat SF-PDI$_2$ film (**Figure 6**). Above 2.6 eV, the absorption is dominated by the MeLPPP donor. The photoluminescence spectrum of the blend, measured in the gated detection mode, is a superposition of fluorescence from SF-PDI$_2$ and a low energy feature with the maximum near 1.6 eV (**Figure 7**a). The latter has to be assigned to a charge transfer transition between the singly occupied LUMO of SF-PDI$_2$ and the singly occupied HOMO of MeLPPP. Such CT states form as a result of photoexciting MeLPPP (SF-PDI$_2$) and subsequent charge transfer from the MeLPPP-LUMO (-HOMO) to the LUMO (HOMO) of an adjacent SF-PDI$_2$ (MeLPPP) chromophore. While the FL of MeLPPP is completely quenched, there is still FL emitted from SF-PDI$_2$. Obviously, there are singlet excitons in the SF-PDI$_2$ domain that are unable to find an accepting site for charge transfer. This can occur when SF-PDI$_2$ is not fully miscible with MeLPPP so that it forms domains of neat SF-PDI$_2$. Such domain formation is a frequently encountered phenomenon in donor–acceptor systems.[55,56]

With increasing delay time there is a continuous transition in overall intensity from SF-PDI$_2$ fluorescence to CT emission, while the shape of both features is basically retained. Plotting the gated emission spectra on a semilogarithmic rather than on linear scale (Figure 7b) demonstrates that both the FL and the CT emission extend into the µs range (in fact, they are noticeable up to 100 µs, see Figure S2, Supporting Information) but their temporal decay is different. While FL decays exponentially with time until DF due to triplet–triplet annihilation takes over at about 20 ns, the CT emission features a power law $I(t) \propto t^n$ with $n \approx -2$ (Figure 7c).

Upon sample cooling the spectral pattern changes. While at room temperature the maxima of the FL and CT emission are independent of delay time (see Figure 7b), there is an increasing redshift of both spectra upon sample cooling to low temperature (see Figure 7d,e). While this is most evident at 5 K, this parallel evolution also prevails at intermediate temperatures (see Figure S2, Supporting Information). The concept of spectral diffusion provides a simple explanation of this observation: When both CT and singlet excitons are not stationary states, their emission spectra should evolve in time. At room temperature both excitations are already equilibrated within the response time of our detection system, but at low temperature their relaxation process is significantly retarded and is amenable to spectral probing. Ultimately, at very long times, the low temperature spectra would approach the room temperature value, indicating that relaxation has been completed, but in practice the excitation decays before this equilibrium is reached.

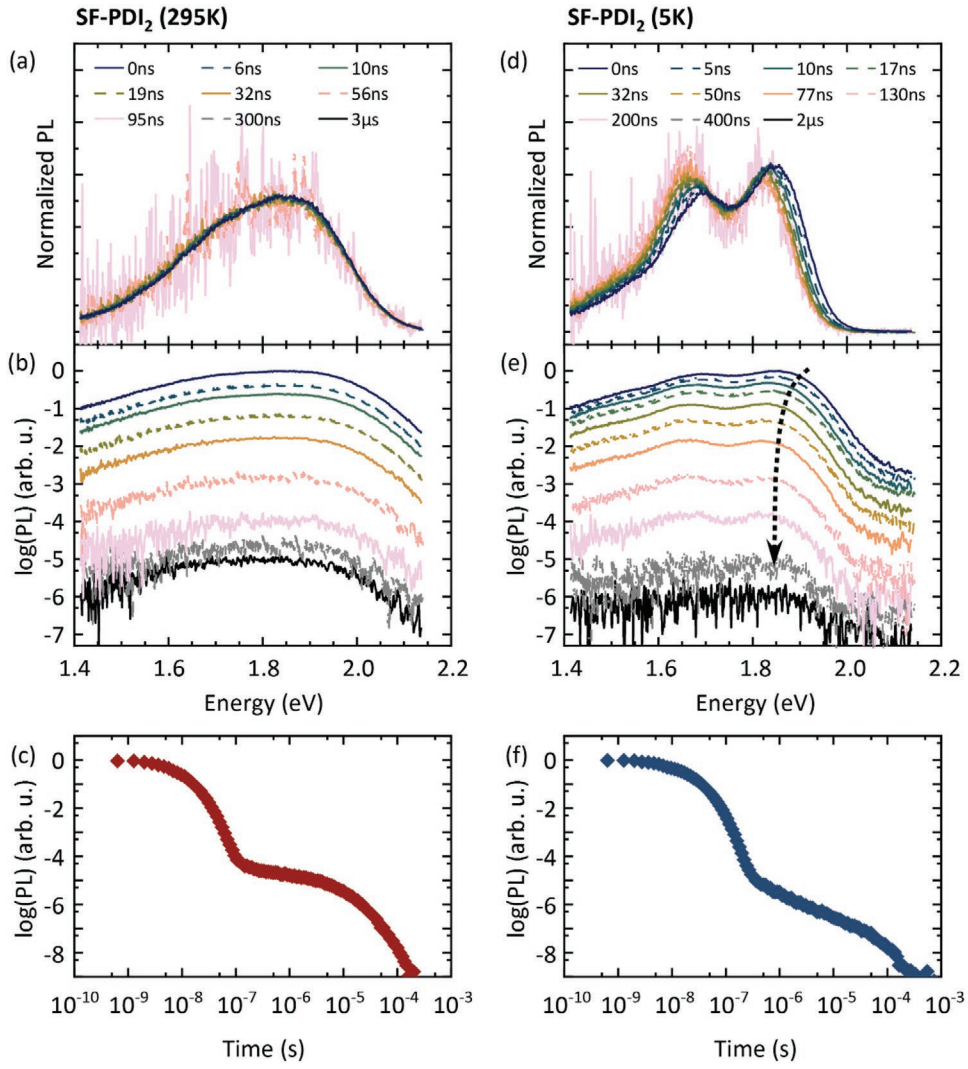

Figure 5. Temporal evolution of the emission for a SF-PDI$_2$ film a–c) at 295 K and d–f) at 5 K. The spectra are normalized to area in panels (a,d), while the relative emission intensities are remained in panels (b,e). Panels (c,f) show the integrated emission intensity as function of decay time on a double logarithmic scale.

The spectral relaxation process is a temperature dependent process and therefore slowed down upon decreasing the temperature. This phenomenon is nicely demonstrated in the neat film (Figure 5). The slowing down of spectral diffusion also explains why CT and FL spectra, probed at a fixed delay time of 106 ns, bear out a blue shift upon sample cooling as shown in **Figure 8** (see Figure S3, Supporting Information for unsmoothed data). In this case the excitations start their journey within the energy landscape at already higher energies. If we deconvolute these spectra into the contributions from the SF-PDI$_2$ singlet state emission and the CT emission, we can fit the CT emission with a single Gaussian lineshape and thus extract the variance, albeit with some considerable experimental uncertainty. The temporal dependence of this variance is displayed in **Figure 9**. Despite the large error bar is nevertheless obvious that σ^2 decreases only weakly upon sample cooling and extrapolates to $\sigma^2 = (8500 \pm 1700)$ (meV)^2 at low temperature. Applying the approach outlined above in the context of Figure 4 we obtain the values summarized in Table 1. From the weak temperature evolution we find that temperature-independent disorder is not only important but rather that it is the dominant source of disorder.

2.3. MeLPPP:PC$_{61}$BM Blends

In our previous work on this subject we reported on the spectroscopy of CT states in MeLPPP:PC$_{61}$BM blends employing the same gated PL techniques as in the current work.[34] We measured the PL spectra of the blends for temperatures between 295 and 5 K within a time domain ranging from ns to 10 µs. Exemplary spectra at 0 and 90 ns can be found in the Figure S4, Supporting Information. Analogous to the blends of MeLPPP with SF-PDI$_2$, we observe that at short delay times there is a superposition of a fluorescence feature and CT emission. The FL component is observed within the entire temperature

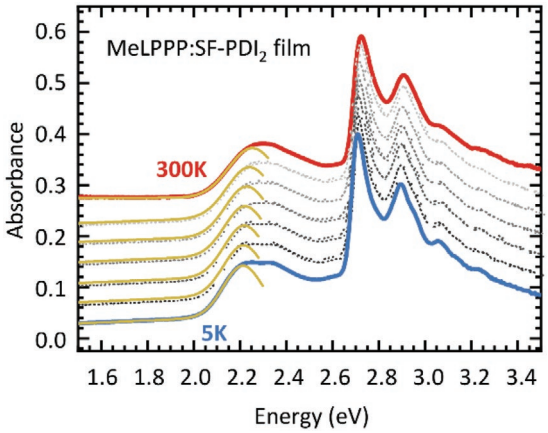

Figure 6. Absorption of a MeLPPP:SF-PDI$_2$ blend film between 300 and 5 K in steps of 50 K. Yellow lines indicate Gaussian fits of the absorption onset of the SF-PDI2 component.

regime and it is identified as delayed FL from the acceptor, that is, the PC$_{61}$BM, caused by triplet–triplet annihilation. It vanishes after 50 ns while only CT emission remains. Different from the results on MeLPPP:SF-PDI$_2$ blends, there is no spectral diffusion upon increasing the delay time. The temporal decay of the CT emission features a power law, $I(t) \propto t^n$ with $n \approx -1.5 - 2.0$. In the course of the current study we determine the evolution of the line shapes of the previously measured CT emission and DF as a function of temperature. The associated variances are shown in Figure 9 While the absolute values are significantly lower than those of the MeLPPP:SF-PDI$_2$ blend, the general pattern of σ^2 versus T is quite similar. For the CT emission, the σ^2 values decrease from 5900 (meV)^2 at 295 K to the asymptotic 5 K value of 3600 (meV)^2 (c.f. Table 1). This implies that in this system also the temperature-independent contribution to the variances of the CT emission exceeds the temperature-dependent contribution.

3. Discussion

In an endeavor to examine the interplay between singlet excitons and CT states in an OSC we studied the time dependent photoluminescence of a neat SF-PDI$_2$ film and a blend of MeLPPP:SF-PDI$_2$ covering a temperature range from 295 K down to 5 K. From fitting Gaussian lineshapes to the spectra at 5 K and at room temperature, we obtained the values for $\sqrt{\sigma^2_{\mathrm{dyn,0K}}+\sigma^2_{\mathrm{stat}}}$ and σ_{tot}, respectively. From these, $\sigma_{\mathrm{dyn,th}}$ was derived using $\sigma^2_{\mathrm{dyn,th}} = \sigma^2_{\mathrm{tot}} - (\sigma^2_{\mathrm{dyn,0K}}+\sigma^2_{\mathrm{stat}})$ as detailed in the paragraph surrounding Equation (2). The results are compared with those of a MeLPPP:PC$_{61}$BM blend. All values are summarized in Table 1.

Before discussing these values and their implications, we briefly comment on the error range given here and indicated in Figures 3,4,9. We estimated our error in the determination of the standard deviation of the Gaussian lineshape fit, that is, the value of $\sqrt{\sigma^2_{\mathrm{dyn,0K}}+\sigma^2_{\mathrm{stat}}}$ and σ_{tot}, generously to be about 10%. All other error ranges follow from the laws of error propagation. As a consequence the relative errors increase from $\sqrt{\sigma^2_{\mathrm{dyn,0K}}+\sigma^2_{\mathrm{stat}}}$ and σ_{tot} to $\sigma_{\mathrm{dyn,th}}$. Our error ranges are on the generous side and may be considered as maximum boundary values. If the standard deviation from the Gaussian fits are considered to be more accurate, this reduces the error range accordingly.

Prior to discussing the actual values of static and dynamic disorder, it is instructive to recall how they impact on the lineshape. Let us consider the case that spectral diffusion does not occur and that the sample is at low temperature. When the spectra are displayed in the form of the reduced absorption (rAbs = Abs · E) and emission (rPL = PL/E), their intercept denotes the position of the 0–0 peak. The key feature is that electron–phonon coupling impacts only on the lineshape below the 0–0 energy. In fact, the emission line becomes a band peaking at an energy λ below the 0–0 position. This is because in the presence of electron–phonon coupling luminescence is accompanied by the emission of low-energy phonons (phonon wing), thus the luminescence band can only be lower than the 0–0 transition energy. Conversely, for absorption, the lineshape is affected above the 0–0 energy by the phonon wing. In contrast to this, static disorder results in an inhomogeneous broadening that is characterized by a Gaussian lineshape, and thus affects the lineshape below and above the 0–0 energy. **Figure 10** illustrates this focusing on the emission lineshape, and more detail is given in the Supporting Information. It is worth pointing out that in a more theoretical description, the phonon wing can also be expressed as a "zero-point vibration" effect. When spectral diffusion takes place, the emitting chromophore is at lower energy to the absorbing chromophore, leading to an energetic displacement between the 0–0 lines of absorption and emission that needs to be added (c.f. Equation (1) above).

Having explored the effects that static and dynamic disorder have on the spectral lineshape, we can already reflect on the values obtained from analyzing the temporal evolutions of the lineshapes as summarized in Table 1 as well as in **Table 2** further below. Regarding the thermal dynamic disorder, $\sigma_{\mathrm{dyn,th}}$, we find a smaller value for the ground states, (60 ± 18 meV, obtained from evaluating the absorption spectra of the singlet state in SF-PDI$_2$), than for the excited states (104 ± 12 meV, derived from analyzing the PL spectra). We attribute this to differences in the molecular geometry and interaction with the environment. In particular, we recall that an excited state is characterized by more occupied antibonding orbitals and correspondingly lesser occupied bonding orbitals than a ground state. Correspondingly, we expect this to soften the molecular skeleton so that low-energy intra-molecular modes become more prevalent. Further, the usually more polar character of an excited state that is based on a π–π^* transition can also be expected to give rise to stronger inter-molecular low-energy phonon modes.

While the analysis of the temperature dependent absorption and emission linewidth allows distinguishing between the disorder present in the 0 K limit and the thermally activated part of the disorder, these data alone do not allow differentiating between the static disorder and the dynamic disorder at 0 K. One approach to disentangle these two contributions would be site selective photoluminescence measurements close to 0 K, such as 5–10 K. When using a narrow-band laser and exciting at the very tail of the DOS, only chromophores resonant with the laser are excited and emit, as spectral diffusion is precluded for tail states. This excludes static disorder, so that the remaining

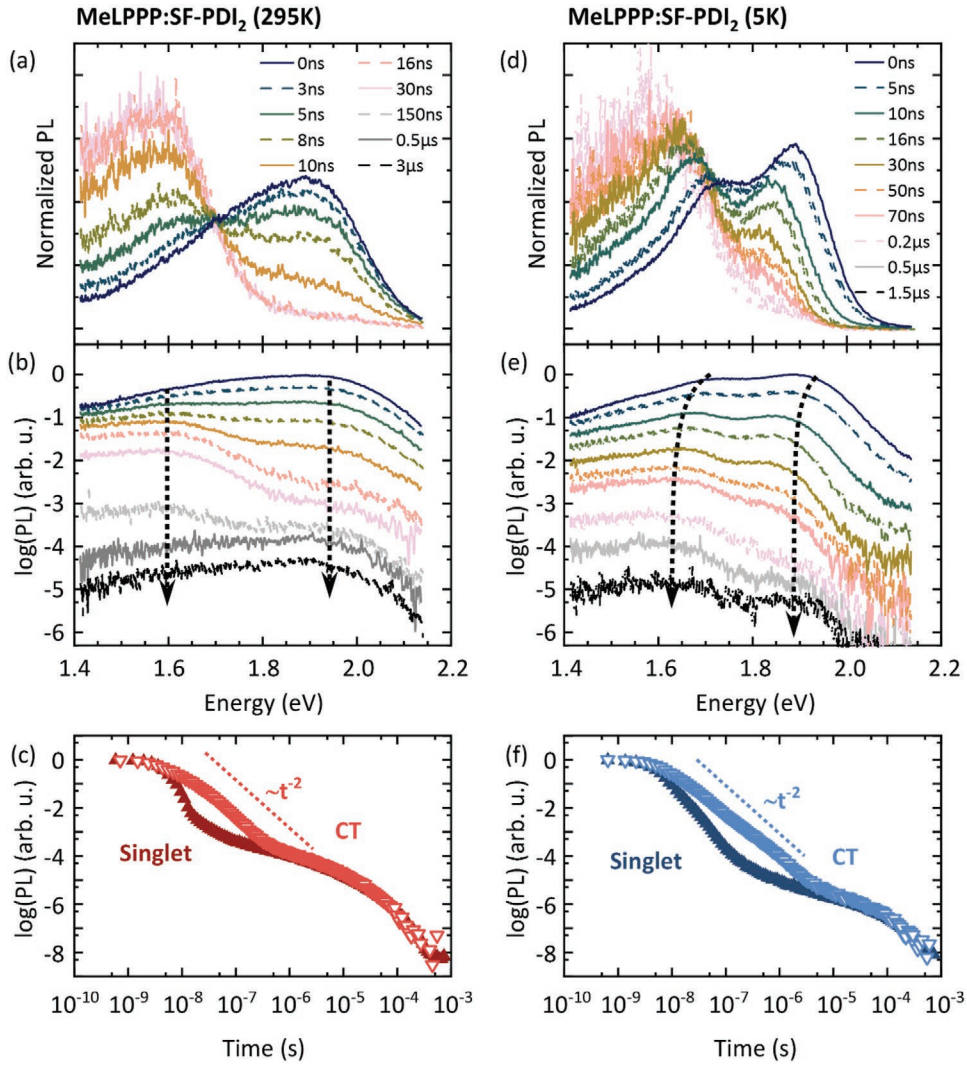

Figure 7. Temporal evolution of the emission for a 1:1 MeLPPP:SF-PDI$_2$ blend film a–c) at 295 K and d–f) at 5 K. The spectra are normalized to area in panels (a,d), while the relative emission intensities are remained in panels (b,e). The dashed lines in (b,e) illustrate the lack (at 295 K) and presence (at 5 K) of spectral diffusion of the fluorescence and CT emission. Panels (c,f) show the integrated emission intensity as function of decay time on a double logarithmic scale. The singlet contribution is integrated between 1.78 and 2.14 eV, the CT contribution is integrated between 1.45 and 1.65 eV.

line width reflects the dynamic disorder present, that is, $\sigma_{dyn.0K}$. Such measurements are beyond the scope of the current work, which focusses on the role of spectral diffusion in the linewidth, but would certainly be of value for a future dedicated study. Site-selective measurements have, however, been carried out by Melianas and co-workers[38] for various donors blended with PCBM as well as for the neat donor films. Their study, detailed in the Supporting Information, comprises 6 common donors (APFOgreen9, rr-P3HT, TQ1, PCDTBT, APFO3, and MDMO-PPV) and PC$_{61}$BM or PC$_{71}$BM as acceptor. For the samples that were excited resonantly, the linewidth at 7 K is about 30 ± 3 meV for S_1 states in the neat films and about 45 ± 5 meV for CT states in the blends. Given the small variation in the values between the different compounds, we can use this as approximate value for $\sigma_{dyn.0K}$ in our sample to provide an estimate for σ_{stat} and also the total σ_{dyn} at 300 K. The resulting values are summarized in Table 2.

This analysis has three implications. First, the analysis suggests that static disorder is a major contribution to the overall disorder and an important factor when analyzing CT states provided that the dynamic disorder at 0 K in our compounds is comparable to that determined by Melianas et al.[38] in their site-selective excitation study on various donors and fullerenes. This requires experimental verification. Second, σ_{stat} is much higher in MeLPPP:SF-PDI$_2$ blends compared to MeLPPP:PC$_{61}$BM. This is plausible due the more ordered acceptor domains in blends based on PC$_{61}$BM as an acceptor. Third, values for σ_{stat} are seemingly much smaller when derived from PL spectra compared to values derived from absorption. As already stated in Section 2.1 above, this is due to the fact that PL usually takes place before reaching thermal equilibrium in the DOS. Thus, the values for σ_{stat} are underestimated, and those for $\sigma_{dyn,th}$ are overestimated.

Regarding our previous results on the MeLPPP:PC$_{61}$BM system, Tvingstedt et al. argued that in view of the rigidity of its

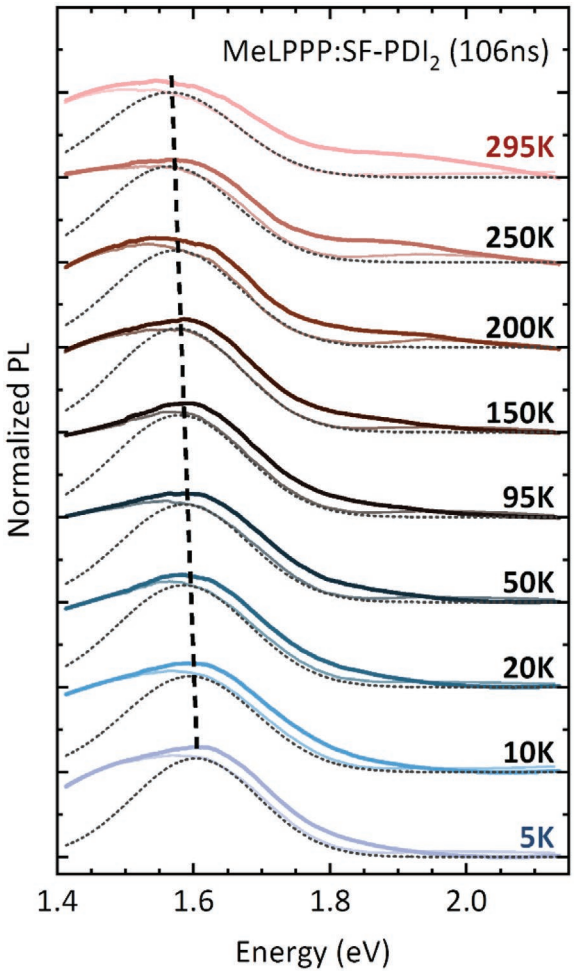

Figure 8. Emission spectrum of a MeLPPP:SF-PDI_2 blend film, recorded at a fixed delay time of 106 ns at different temperatures. Contributions from neat SF-PDI_2, centered at 1.85 eV, are separated and the remaining emission of the CT state is shown in lighter colors with a Gaussian fit. The dashed line indicates the spectral shift of the CT state. Spectra are smoothed using a Savitzky–Golay filter (for unprocessed spectra see Figure S3, Supporting Information).

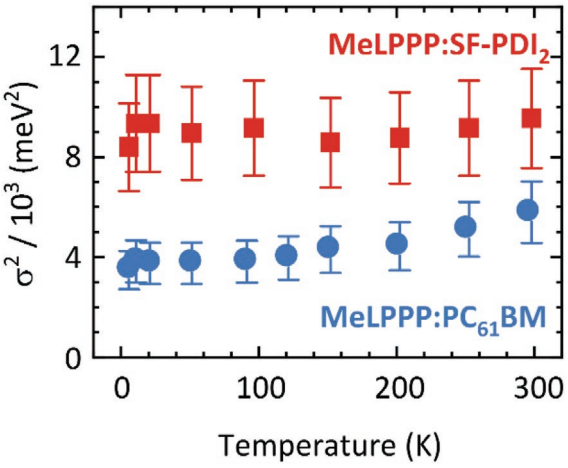

Figure 9. Squared Gaussian linewidths σ^2 of the CT emission 100 ns after excitation as a function of temperature for a MeLPPP:SF-PDI_2 blend film (red) and a MeLPPP:$PC_{61}BM$ blend film (blue).

backbone, MeLPPP is not a representative donor material and therefore a general conclusion drawn from an individual system is doubtful. MeLPPP is indeed special because the rigidity of the backbone translates into an unusually narrow experimental S_1–S_0 0–0 line both in absorption and FL ($\sigma \approx 25 - 35$ meV). Quantum chemical calculations confirm that their widths are caused by structural disorder that persists down to 0 K.[40] On the other hand, the absorption spectra of films of the classic conjugated polymer MEH-PPV also bear out a virtually temperature independent Gaussian line width of 80 meV.[54] This demonstrates that loss of the rigidity of the backbone can increase static disorder to the extent that dynamic disorder becomes less important. Since efficient OSCs are based on blended films whose components form clusters of non-rigid donors and acceptors that feature significant inhomogeneous line-broadening, we expect that static disorder is, in fact, important to understand the dynamics of CT states in OSCs. This is in correspondence with the most recent theoretical study by Yan et al.[57] and the experimental work by Upreti et al.[39] who reinforce not only the claim concerning the importance of static disorder in the description of CT states in OSCs itself but stress its relevance for the open-circuit voltage of CT states.

From the temperature dependences of the absorption and FL spectra of the neat SF-PDI_2 film as well as from their evolution on time we learn that generated singlet excitons execute a random walk within their DOS distribution and suffer spectral diffusion (c.f. Figure 5) before they decay radiatively or non-radiatively. This spectral diffusion is reflected in the Stokes shift between absorption and FL. While spectral diffusion is a well-known ensemble effect in bulk chromophores, its relevance for an OSC has not been duly appreciated. The fact that the CT emission from a MeLPPP:SF-PDI_2 blend bears out the same temporal red-shift of FL emitted from either a neat SF-PDI_2 film or a blend tells us that both emissions are correlated. This symbatic temporal evolution of fluorescence and CT emission of the MeLPP:SF-PDI_2 blend, documented in Figure 7 provides a handle on the dynamics of the CT states. Upon photogenerating a singlet exciton on a SF-PDI_2 acceptor within a SF-PDI_2 domain, this excitation executes a random walk, thereby

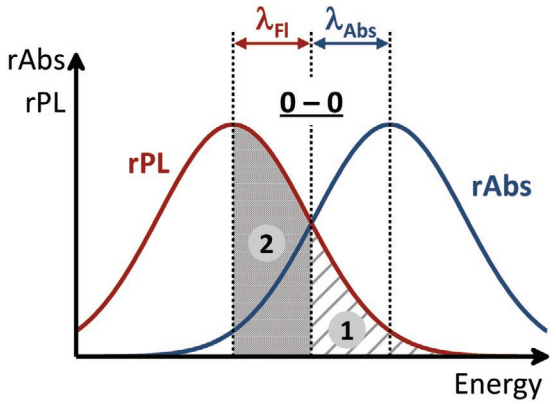

Figure 10. Contribution of 1) static and 2) dynamic disorder to the total linewidth and the Stokes' shift for CT state emission. Note that the two contributions are convoluted and do NOT add linearly.

Table 2. Overview of the disorder values at 300 and 0 K.

	$\sigma^2_{dyn,0K}$ [a)] [10^3 (meV)^2]	σ^2_{stat} [b)] [10^3 (meV)^2]	$\sigma^2_{dyn,th}$(300 K) [c)] [10^3 (meV)^2]	σ^2_{dyn}(300 K) [d)] [10^3 (meV)^2]	σ^2_{tot}(300 K) [c)] [10^3 (meV)^2]	$\sigma_{dyn,0K}$ [a)] [meV]	σ_{stat} [meV]	σ_{dyn} (300 K) [meV]	σ_{tot}(300 K) [meV]	$\frac{\sigma_{stat}}{\sigma_{dyn}(300\,K)}$
SF-PDI$_2$ S1 Abs in neat film	0.9 ± 0.2	5.3 ± 1.3	2.7 ± 2.2	3.6 ± 2.2	8.9 ± 1.8	30 ± 3	73 ± 9	60 ± 18	94 ± 9	1.2 ± 0.4
SF-PDI$_2$ S1 PL in neat film	0.9 ± 0.2	1.4 ± 0.5	10.0 ± 2.5	10.9 ± 2.5	12.3 ± 2.5	30 ± 3	37 ± 7	104 ± 12	111 ± 11	0.4 ± 0.1
SF-PDI$_2$ S1 Abs in MeLPPP:SF-PDI$_2$	0.9 ± 0.2	6.1 ± 1.4	3.4 ± 2.5	4.4 ± 2.5	10.4 ± 2.1	30 ± 3	78 ± 9	66 ± 19	102 ± 10	1.2 ± 0.4
CT state PL in MeLPPP:SF-PDI$_2$	2.0 ± 0.5	6.5 ± 1.8	1.1 ± 1.1	3.1 ± 2.6	9.6 ± 2.0	45 ± 5	81 ± 11	56 ± 23	98 ± 10	1.4 ± 0.6
CT state PL in MeLPPP:PC$_{61}$BM	2.0 ± 0.5	1.6 ± 0.8	2.3 ± 1.4	4.3 ± 1.5	5.9 ± 1.2	45 ± 5	40 ± 11	66 ± 11	77 ± 8	0.6 ± 0.2

[a)]Estimate, based on values for other donors in Ref. [38]; [b)]By subtracting the estimated value of $\sigma^2_{dyn,0K}$ from the measured value of $\sigma^2_{dyn,0K}+\sigma^2_{stat}$ reported in Table 1; [c)]Experimentally measured and reported in Table 1, here for ease of reference; [d)]$\sigma^2_{dyn}\,(300\,K)=\sigma^2_{dyn,0K}+\sigma^2_{dyn,th}(300\,K)$.

relaxing energetically within the SF-PDI$_2$ domain as illustrated in Figure 7b,e. In the course of their journey they can either generate a CT state at the interface to the donor domain or they decay radiatively. The correlation between the redshifts of the FL of the SF-PDI$_2$ and the CT emission suggests that the generated CT states reflect the position within the energy landscape at which they have been created. The thus-generated CT state may or may not relax further, yet the essential spectral diffusion involved with the CT state emission has already occurred within the SF-PDI$_2$ domain, that is, prior to the birth of the CT state. In passing we note that the intrinsically low oscillator strength in CT states precludes a significant rate of Förster transfer. Since spectral diffusion depends on static disorder and is slowed down at lower temperatures, it may already be completed with the response time of the experimental set-up (see Figure 7a,b). From the associated distribution of CT energies it follows that CT states are therefore not well defined entities and can therefore not appropriately be treated with an approach that neglects their statistical variation in an ensemble. The generated CT states reflect their generation and the course of spectral diffusion of the precursor singlet excitons yet not—or only marginally—subsequent CT state diffusion. The fact that the PL of an OSC blend contains an FL component can be taken as indication for domain formation in the blend. Moreover, the observation of the two distinct bands allows for a further conclusion. It implies that the CT state emission cannot be assigned to a hybrid CT-state that would be degenerate with the singlet state. Frequently, the PL spectra of blends with NFAs feature emission spectra that are identical with the FL spectra of one of their components.[55,56,58] Based upon the current work we suggest that due care must be taken to avoid mistakenly assigning such bands to hybrid CT-states when acceptor domain formation might prevail.[59] Singlet state emission from within acceptor domains can mask a weak lower-energy CT emission, in particular when that CT emission is at the limit of the detectors spectral range and sensitivity and when it is weak due to the energy gap law.[43]

4. Conclusions

Upon optical excitation of a MeLPPP:SF-PDI blend or of a MeLPPP:PC$_{61}$BM blend, CT states are produced via relaxed singlet states within acceptor domains. They carry a memory of their time and temperature dependent generation but are more or less stationary afterward. Therefore the absence of a significant shift of the CT emission cannot be taken as evidence that static disorder is unimportant as Göhler et al. argued based upon the missing temperature dependent shift of the CT peak in an electroluminescence experiment.[36] Rather, for both, optical as well as electrical generation, the emitting CT states have been generated from singlet states that had already suffered energetic relaxation. In case of optical generation the generation occurs through charge transfer from the relaxed singlet state, and in the case of electrical excitation CT states are generated through the recombination of electrons and holes that had executed an energy dissipating random walk within the energy landscape on the blend. Hence, the energy gap between the maximum of the CT state absorption—as determined from fitting tail of the EQE spectrum of a solar cell—and the maximum of the CT emission spectrum does not give a measure for the loss of spectral energy that would be associated with static disorder, for example, by CT state spectral diffusion. Rather, this Stokes' shift only reflects the dynamic disorder, that is, 2λ. In other words, in contrast to singlet excitons in a donor or acceptor domain, for CT states, the lack of any significant further spectral diffusion changes Equation (1) to

$$\Delta E = E^{Abs}_{0-0} - E^{PL}_{0-0} = \lambda_{abs} + \lambda_{Fl} \tag{3}$$

This is an important notion to recognize. This is consistent with the spectral analysis of the CT-spectrum and the EQE spectrum as detailed in the work of Kahle et al.[34] The linewidth of the emission spectrum of the CT states is controlled by both static and dynamic disorder, while the Stokes' shift only reflects the reorganization energy.[34] This may appear paradox at first sight yet is easily resolved when recalling that the crossing point of the emission and absorption of the CT state, displayed as reduced absorption and reduced PL, defines the 0–0 position. Thus, any line broadening of the low-temperature PL at energies above that 0–0 position arises from static disorder, while that below is from dynamic disorder, that is, low-frequency phonon modes, as illustrated in Figure 10. Even though CT states are subject to dynamic disorder which is reflected in their

Stokes's shift, their linewidth also carries the signature of the static disorder from the ensemble in which they are generated.

5. Experimental Section

The materials used for the experiments were MeLPPP, SF-PDI_2, and $PC_{61}BM$ (Figure 1). The methylated ladder-type poly(*para*-phenylene) polymer MeLPPP with average molecular weights M_n/M_w of 37/82 kDa was synthesized as described in the literature.[60,61] SF-PDI_2 was purchased from 1-materials, and $PC_{61}BM$ was obtained from Sigma Aldrich and used without further purification. Roughly 100 nm thick films of a blend of MeLPPP and SF-PDI_2 were spun from chloroform solution (15 mg mL^{-1}). For time-gated emission spectroscopy, the sample was excited by a frequency-tripled Nd-YAG laser (Innolas SpitLight 600) with a wavelength of 355 nm (3.5 eV) and pulse width of 7 ns. Emission spectra with distinct delay and integration time were acquired using an intensified charge coupled device camera (Andor iStar 334), which was triggered by the laser. Delay and integration time were exponentially increased up to the sub-ms range to account for decreasing emission intensity at later times. The PL decay transients were corrected for this increase in integration time. All experiments were performed with the sample being kept in a temperature controlled continuous flow helium cryostat (Oxford Instruments OptistatCF).

Supporting Information

Supporting Information is available from the Wiley Online Library or from the author.

Acknowledgements

The authors acknowledge financial support by the Bavarian State Ministry of Science, Research, and the Arts (StMWK) through the Collaborative Research Network "Solar Technologies go Hybrid." This research was also supported by EU Marie Skłodowska-Curie ITN TADF*life* grant (Grant agreement no. 812872). S.W. was supported by the Elite Network Bavaria (ENB) in the framework of the Elite Study Program "Macromolecular Science" and "MINT Lehramt plus". S.B. acknowledges funding by the Deutsche Forschungsgemeinschaft, DFG, through the grant "MARS," Grant no. 03462892.

Open access funding enabled and organized by Projekt DEAL.

Conflict of Interest

The authors declare no conflict of interest.

Data Availability Statement

The data that support the findings of this study are available from the corresponding author upon reasonable request.

Keywords

donor–acceptor blends, inhomogeneous line broadening, non-fullerene acceptors, photoluminescence-linewidth, spectral diffusion

Received: October 1, 2021
Revised: January 28, 2022
Published online: February 27, 2022

[1] J. Kurpiers, T. Ferron, S. Roland, M. Jakoby, T. Thiede, F. Jaiser, S. Albrecht, S. Janietz, B. A. Collins, I. A. Howard, D. Neher, *Nat. Commun.* **2018**, *9*, 2038.
[2] K. Vandewal, S. Albrecht, E. T. Hoke, K. R. Graham, J. Widmer, J. D. Douglas, M. Schubert, W. R. Mateker, J. T. Bloking, G. F. Burkhard, A. Sellinger, J. M. J. Fréchet, A. Amassian, M. K. Riede, M. D. McGehee, D. Neher, A. Salleo, *Nat. Mater.* **2014**, *13*, 63.
[3] T. Unger, S. Wedler, F.-J. Kahle, U. Scherf, H. Bässler, A. Köhler, *J. Phys. Chem. C* **2017**, *121*, 22739.
[4] Y. Zhong, M. Causa, G. J. Moore, P. Krauspe, B. Xiao, F. Günther, J. Kublitski, R. Shivhare, J. Benduhn, E. BarOr, S. Mukherjee, K. M. Yallum, J. Réhault, S. C. B. Mannsfeld, D. Neher, L. J. Richter, D. M. DeLongchamp, F. Ortmann, K. Vandewal, E. Zhou, N. Banerji, *Nat. Commun.* **2020**, *586*, E11.
[5] H. Bässler, A. Köhler, *Phys. Chem. Chem. Phys.* **2015**, *17*, 28451.
[6] L. E. de Sousa, V. Coropceanu, D. A. da Silva Filho, G. Sini, *Adv. Theory Simul.* **2020**, *3*, 1900230.
[7] S. M. Menke, A. Cheminal, P. Conaghan, N. A. Ran, N. C. Greehnam, G. C. Bazan, T.-Q. Nguyen, A. Rao, R. H. Friend, *Nat. Commun.* **2018**, *9*, 277.
[8] S. Athanasopoulos, S. Tscheuschner, H. Bässler, A. Köhler, *J. Phys. Chem. Lett.* **2017**, *8*, 2093.
[9] S. Athanasopoulos, F. Schauer, V. Nádaždy, M. Weiß, F.-J. Kahle, U. Scherf, H. Bässler, A. Köhler, *Adv. Energy Mater.* **2019**, *9*, 1900814.
[10] P. K. Nayak, K. L. Narasimhan, D. Cahen, *J. Phys. Chem. Lett.* **2013**, *4*, 1707.
[11] F. Gao, W. Tress, J. Wang, O. Inganäs, *Phys. Rev. Lett.* **2015**, *114*, 128701.
[12] A. A. Bakulin, Y. Xia, H. J. Bakker, O. Inganäs, F. Gao, *J. Phys. Chem. C* **2016**, *120*, 4219.
[13] X.-K. Chen, V. Coropceanu, J.-L. Brédas, *Nat. Commun.* **2018**, *9*, 5295.
[14] A. P. Arndt, M. Gerhard, A. Quintilla, I. A. Howard, M. Koch, U. Lemmer, *J. Phys. Chem. C* **2015**, *119*, 13516.
[15] R. A. Marcus, *Discuss. Faraday Soc.* **1960**, *29*, 21.
[16] J. Jortner, *J. Chem. Phys.* **1976**, *64*, 4860.
[17] V. G. Levich, in *Advances in Electrochemistry and Electrochemical Engineering*, Vol.4 (Ed: T. Delahay), Wiley, New York **1966**, p. 249.
[18] M. Bixon, J. Jortner, *Adv. Chem. Phys.* **1999**, *106*, 35.
[19] I. R. Gould, D. Noukakis, L. Gomez-Jahn, R. H. Young, J. L. Goodman, S. Farid, *Chem. Phys.* **1993**, *176*, 439.
[20] R. A. Marcus, N. Sutin, *Biochim. Biophys. Acta, Bioenerg.* **1985**, *811*, 265.
[21] G. L. Closs, J. R. Miller, *Science* **1988**, *240*, 440.
[22] S. Fukuzumi, K. Ohkubo, H. Imahori, D. M. Guldi, *Chem. - Eur. J.* **2003**, *9*, 1585.
[23] H. Bässler, *Phys. Status Solidi B* **1993**, *175*, 15.
[24] G. Aydin, I. Yavuz, *J. Phys. Chem. C* **2021**, *125*, 6862.
[25] Z. Zheng, N. R. Tummala, T. Wang, V. Coropceanu, J.-L. Brédas, *Adv. Energy Mater.* **2019**, *9*, 1803926.
[26] T. Linderl, T. Zechel, A. Hofmann, T. Sato, K. Shimizu, H. Ishii, W. Brütting, *Phys. Rev. Appl.* **2020**, *13*, 024061.
[27] I. Rörich, O. V. Mikhnenko, D. Gehrig, P. W. M. Blom, N. I. Crăciun, *J. Phys. Chem. B* **2017**, *121*, 1405.
[28] R. Coehoorn, P. A. Bobbert, H. van Eersel, *Phys. Rev. B* **2019**, *99*, 024201.
[29] H. Bässler, A. Köhler, *Top. Curr. Chem.* **2012**, *312*, 1.
[30] A. Devižis, A. Serbenta, K. Meerholz, D. Hertel, V. Gulbinas, *Phys. Rev. Lett.* **2009**, *103*, 027404.
[31] A. Melianas, M. Kemerink, *Adv. Mater.* **2019**, *31*, 1806004.
[32] T. Upreti, Y. Wang, H. Zhang, D. Scheunemann, F. Gao, M. Kemerink, *Phys. Rev. Appl.* **2019**, *12*, 064039.
[33] T. M. Burke, S. Sweetnam, K. Vandewal, M. D. McGehee, *Adv. Energy Mater.* **2015**, *5*, 1500123.

[34] F.-J. Kahle, A. Rudnick, H. Bässler, A. Köhler, *Mater. Horiz.* **2018**, *5*, 837.
[35] K. Tvingstedt, J. Benduhn, K. Vandewal, *Mater. Horiz.* **2020**, *7*, 1888.
[36] C. Göhler, M. Saladina, Y. Wang, D. Spoltore, J. Benduhn, K. Leo, C. Deibel, *Phys. Rev. Appl.* **2021**, *15*, 064009.
[37] M. Panhans, S. Hutsch, J. Bendhun, K. S. Schellhammer, V. C. Nikolis, T. Vangerven, K. Vandewal, F. Ortmann, *Nat. Commun.* **2020**, *11*, 1488.
[38] A. Melianas, N. Felekidis, Y. Puttisong, S. C. J. Meskers, O. Inganäs, W. M. Chen, M. Kemerink, *Proc. Natl. Acad. Sci. U. S. A.* **2019**, *116*, 23416.
[39] T. Upreti, S. Wilken, H. Zhang, M. Kemerink, *J. Phys. Chem. Lett.* **2021**, *12*, 9874.
[40] M. Marcus, J. D. Milward, A. Köhler, W. Barford, *J. Phys. Chem. A* **2018**, *122*, 3621.
[41] H. Bässler, D. Kroh, F. Schauer, V. Nádaždy, A. Köhler, *Adv. Funct. Mater.* **2021**, *31*, 2007738.
[42] W. Siebrand, *J. Chem. Phys.* **1967**, *46*, 440.
[43] G. Londi, S.-U.-Z. Khan, L. Muccioli, G. D'Avino, B. P. Rand, D. Beljonne, *J. Phys. Chem. Lett.* **2020**, *11*, 10219.
[44] O. V. Mikhnenko, F. Cordella, A. B. Sieval, J. C. Hummelen, P. W. M. Blom, M. A. Loi, *J. Phys. Chem. B* **2008**, *112*, 11601.
[45] S. C. J. Meskers, J. Hübner, M. Oestreich, H. Bässler, *J. Phys. Chem. B* **2001**, *105*, 9139.
[46] B. Movaghar, M. Grünewald, B. Ries, H. Bassler, D. Würtz, *Phys. Rev. B* **1986**, *33*, 5545.
[47] J. Sperling, F. Milota, A. Tortschanoff, C. Warmuth, B. Mollay, H. Bässler, H. F. Kauffmann, *J. Chem. Phys.* **2002**, *117*, 10877.
[48] N. Banerji, S. Cowan, M. Leclerc, E. Vauthey, A. J. Heeger, *J. Am. Chem. Soc.* **2010**, *132*, 17459.
[49] G. R. Hayes, I. D. W. Samuel, R. T. Phillips, *Phys. Rev. B* **1995**, *52*, R11569.
[50] S. A. Schmid, K. H. Yim, M. H. Chang, Z. Zheng, W. T. S. Huck, R. H. Friend, J. S. Kim, L. M. Herz, *Phys. Rev. B* **2008**, *77*, 115338.
[51] S. Athanasopoulos, S. T. Hoffmann, H. Bässler, A. Köhler, D. Beljonne, *J. Phys. Chem. Lett.* **2013**, *4*, 1694.
[52] S. T. Hoffmann, E. Scheler, J.-M. Koenen, M. Forster, U. Scherf, P. Strohriegl, H. Bässler, A. Köhler, *Phys. Rev. B* **2010**, *81*, 165208.
[53] R. S. Sánchez-Carrera, P. Paramonov, G. M. Day, V. Coropceanu, J.-L. Brédas, *J. Am. Chem. Soc.* **2010**, *132*, 14437.
[54] S. T. Hoffmann, H. Bässler, A. Köhler, *J. Phys. Chem. B* **2010**, *114*, 17037.
[55] J. Liu, S. Chen, D. Qian, B. Gautam, G. Yang, J. Zhao, J. Bergqvist, F. Zhang, W. Ma, H. Ade, O. Inganäs, K. Gundogdu, F. Gao, H. Yan, *Nat. Energy* **2016**, *1*, 16089.
[56] L. Perdigón-Toro, L. Q. Phuong, S. Zeiske, K. Vandewal, A. Armin, S. Shoaee, D. Neher, *ACS Energy Lett.* **2021**, *6*, 557.
[57] J. Yan, E. Rezasoltani, M. Azzouzi, F. Eisner, J. Nelson, *Nat. Commun.* **2021**, *12*, 3642.
[58] D. Qian, Z. Zheng, H. Yao, W. Tress, T. R. Hopper, S. Chen, S. Li, J. Liu, S. Chen, J. Zhang, X.-K. Liu, B. Gao, L. Ouyang, Y. Jin, G. Pozina, I. A. Buyanova, W. M. Chen, O. Inganäs, V. Coropceanu, J.-L. Bredas, H. Yan, J. Hou, F. Zhang, A. A. Bakulin, F. Gao, *Nat. Mater.* **2018**, *17*, 703.
[59] K. Vandewal, S. Mertens, J. Benduhn, Q. Liu, *J. Phys. Chem. Lett.* **2020**, *11*, 129.
[60] U. Scherf, K. Müllen, *Makromol. Chem. Rapid Comm.* **1991**, *12*, 489.
[61] U. Scherf, A. Bohnen, K. Müllen, *Makromol. Chem.* **1992**, *193*, 1127.